Investigating the effect of thermal stresses on Multijunction PV solar cells

Reem H Ahmed[1], I El-Mahallawi[1,2] and Mahmoud Tash[2]
[1] Faculty of Engineering, Department of Mechanical Engineering, The British University in Egypt, El-Sherouk City, Cairo 11837, Egypt
[2] Mining, Petroleum, and Metallurgical Engineering Dept., Faculty of Engineering, Cairo University, Giza, 12613, Egypt
E-mail: reem157226@bue.edu.eg

Abstract. Multijunction Photovoltaics (MJPV) technologies represent a field of robust research aimed at enhancing photovoltaic efficiencies. Perovskite, GaAs, and GaN semiconductors with organic substrates are suitable for multi-junction solar cells due to their ease, efficiency, and cost-effectiveness in deposition on the active layers of silicon solar cells. Thermal stresses arise at the manufacturing and operational temperatures of Si/indium/perovskite, Si/indium/GaN, and Si/indium/GaAs multijunction photovoltaic cells due to thermal mismatch. This work aims to evaluate the effects of thermal loading on a multi-junction system composed of perovskite, GaAs, and GaN particles on silicon, utilising finite element analysis software (ABAQUS) and representative volume elements (RVE). One method experienced reduced stress compared to the other because of the differing material properties. Moreover, the GaAs region of model (C) experiences the highest level of stress. Quantitative analysis indicated that the Model C, that includes GaAs as upper layer, exhibited the highest thermal stress concentration at 48MPa, notably exceeding the other models; for instance, Model B with GaN recorded a peak stress of 45.5 MPa, while Model A displayed a maximum stress of 41 MPa in the indium section. These findings highlight the influence of material characteristics on stress distribution in multijunction solar cells. Future research will examine the impact of different thermal configurations relevant to the operational conditions of solar panels and utilise the Embedded Void Approach (EVA) to mitigate dislocation propagation induced by elevated thermal stresses.

1. Introduction

Over the last few decades, silicon has shown to be exceptionally reliable and meets the lifetime requirements of most photovoltaic solar cell applications. Given that silicon is an abundant element on Earth, there is enough supply of raw materials for its extraction. Moreover, the wavelength range of the crystalline silicon solar cell varies from 300 to 1200 nm, and the efficiency for the crystalline silicon solar cell can reach 25.6%, with a practical limit of 27% [1]. Another technology of the solar cell is the single-junction solar cell, and this type is getting closer to the potential maximum efficiency. On the other hand, solar cells employ the GaAs semiconductor material, which presently boasts the highest efficiency in single-junction technology at 28.8% [2]. The theoretical efficiency limit (radiative limit) for the GaAs solar cell can reach approximately 32.5% [3].

The aforementioned information for the single-junction solar cells highlights that its efficiency is limited, and it is essential to enhance the solar cell's effectiveness and reduce the thickness of the

absorption layer in order to make it more economically viable. Therefore, to overcome this issue, researchers introduced a new technology for solar cells, which is the multijunction solar cell. This technology uses a few different absorber materials to collect a broader range of the solar spectrum and is one way to increase the fundamental c-Si cell efficiency constraint. A wider bandgap material, on the other hand, minimises heat carrier losses and boosts solar cell efficiency. Under conventional test settings, in 2017, the potential conversion efficiency for the MJ-PV reached 46% [8][4]. There have been several different tandem solar cell technologies created so far [5–10], and [10]. Furthermore, Tandem cells can achieve efficiencies higher than 50%, which is substantial improvement over single-junction silicon cells. With a perovskite/silicon arrangement, the record efficiency for a tandem solar cell as of 2022 is 29.15% [11]. Meanwhile, the III-V semiconductors, such as InGaAs, AlInP, AlGaInP, GaInP, InP, GaAs, etc., have garnered considerable attention in solar cell technology, especially with MJPV cells, as using III-V semiconductors can enhance the power conversion efficiency (PCE) of more than 40%, surpassing that of other types of solar cells; however, implementing the MJ-PV cells for a large-scale power plant is a hurdle, as the cost will be very high [11],[12].

Over the preceding two decades, researchers have been trying to find an affordable and effective semiconductor material and enhancing the design for MJPV cells to be more efficient. Additionally, subsequent advantages of perovskite ($CH_3NH_3PbI_3$) may elucidate its remarkable photovoltaic characteristics: extended diffusion lengths for charge carriers, non-polar mobility for photon-induced carriers, abundant compositions, and adjustable band gaps ranging from 1.2 to 3.1 eV. Perovskite solar cells (PSC) have been recognised as an appropriate upper sub-cell for tandem or multi-junction configurations due to their tunable band gap, their shorter wavelength spectrum (300–800 nm), and optoelectronic properties, among other aforementioned characteristics. Moreover, the overall photoelectric conversion efficiency of perovskite solar cells (PSC) is 21% [13,14].Furthermore, GaN material, which is commonly used in power amplifiers (PAs) for terrestrial applications, has attracted interest for space applications due to its remarkably high power levels at pertinent frequencies, coupled with minimal losses in passive networks and suboptimal noise performance in receivers [15]. Some recent studies are focused on finding a method to minimise dislocation and other faults in multijunction PV cells that happen as a result of thermal stresses [16–18]. In those studies, ABAQUS software was used to examine the impact of voids on the dislocation propagation and the stresses, and the displacement was used as an indication for the dislocation density. Furthermore, the involvement of the voids in close proximity to the GaAs/Si multijunction solar cell shows a decrease in thermal stresses, which consequently reduces the dislocations. The result shows that the stress in the Si layer reduces by 14% and increases 18% in the GaAs layer, as well as the maximum displacement dropping to 11%. Overall, this approach is a suitable solution for the 1.0 eV sub-cell, which could reach the efficiency of 45% [18].

Moreover, Bagheri et al. [19] conducted a simulation for InGaP/GaAs MJPV with AlGaAs tunnel junction in order to investigate the power conversion efficiency of the MJPV cells by manipulating the window layers and introducing back-surface field layers. The findings show that MJ-PV cells with six tunnel layers of different thicknesses can reach a high PCE of 35.5% when InAlGaP is used in the back-surface field and window layer. In addition, the PCE was improved to 36.24% by increasing the thickness of the rear surface field layer of the top cell.

As previously stated, MJPV cells have the ability to exceed silicon single-junction solar cells' intrinsic efficiency limit. However, silicon can still be useful as a bottom junction and substrate material in these solar cells. This feature is alluring because the majority of thin-film absorbers necessitate a support structure due to their inadequate thickness for independent stability. Silicon possessing a bandgap of 1.1 eV is highly appropriate for dual-junction and triple-junction devices. The ideal bandgap energy for adding an additional absorber atop silicon is 1.7 eV; for two absorbers in series, it is 2.0 eV, and for two absorbers in parallel, it is 1.5 eV. The exact bandgaps depend on several factors, including the long-wavelength response of the silicon-bottom solar cell and the transparency of the upper layers. This seems to be a substantial challenge in the fabrication of tandem solar cells on

silicon. To facilitate the deposition of planar thin-film absorbers on the front, the light-trapping features must be repositioned from the front side to the rear of the wafer [20–22]. One method to accomplish this is by integrating a pyramid texture, spheres, or nanostructured grating on the posterior surface of the silicon wafer. This will effectively extend the light path through the silicon, leading to enhanced absorption at the indirect bandgap [23–25].

Lastly, Soma and Mohammad [26] used the finite element method (FEM) to simulate a three-dimensional planar perovskite solar cell. The suggested device is comprehensively described with an optical-electrical hybrid modelling technique. To validate the proposed version, it is essential to compare it with experimental results. The incorporation of a secondary absorber layer made of $CH_3NH_3SnI_3$ improves the architecture of a perovskite solar cell that depends exclusively on $CH_3NH_3PbI_3$. Despite the $CH_3NH_3SnI_3$ layer being roughly 200 nanometres in thickness, the recent collaboration has elevated the PCE from approximately 14.32 percent to around 15.32 percent. Applying a 40 nm MgF_2 coating, which serves as an anti-reflective agent, to a surface with a designated percentage can boost the short circuit current (Jsc). Upon evaluating the findings of the anti-find reflectors, the succeeding allocation will be regularly modified in the future. Substituting the flat back layer with a regularly corrugated decreasing back layer and the anti-reflector with a dynamic layer might yield a PCE of 17.5%, representing the proposed photovoltaic cell configuration (PCC) for this innovation.

The aforementioned studies highlighted that the use of MJPV cells combined with GaAs or $CH_3NH_3PbI_3$ with a silicon substrate has the potential to increase the solar cell efficiency and can be used in space applications. Still, at the same time, there is a probability that a thermal stress occurs in those cells, which is a critical issue, as it causes dislocation in the cells that may propagate and cause cracks in the cells. In addition, a study found that the efficiency of GaN solar cells can reach 20% [27]. Therefore, investigating and understanding the impact of thermal stress on these cells is essential in order to enhance their thermal stability. The thermal stress can also cause dislocations in the cells, which will spread and lead to a crack in the cell. This will make the MJPV cell even less long-lasting and effective [27].

Although the potential efficiency for the MJPV cells is higher than the conventional solar still, it is still challenging to reach the thermal stability for the MJPV cell under different environmental conditions. Moreover, the previous studies didn't focus on investigating the effect of different operating temperatures on MJPV, especially for materials with a high potential efficiency such as GaN, perovskite, and GaAs. So, the aim of this paper is to look into how the operating temperature affects the distribution of thermal stress across the MJPV cell structure and at the interface between the layers. This will be done using finite element analysis (FEM) and thermoelasticity-based constitutive equations. Furthermore, this study will provide a foundation for further elastic/plastic simulation of MJPV cells and investigate the potential of organic-based perovskite, GaN, and GaAs as a top cell, with indium as the middle cell and silicon as a substrate. This will be integrated with the finite element method (FEM) to model a periodic representative volume element (RVE) for Si/Indium/perovskite, Si/Indium/GaN, and Si/Indium/GaAs multijunction photovoltaic cells. This study will utilise finite-element software (ABAQUS) to analyse the outcomes of these models.

2. Theoretical Model

Three models have been created, all with identical geometry and materials, except for the top layer, which varied in material composition across each model. Figure 1 shows the structure of Model (A), which consisted of a silicon base layer, an indium mid-sphere, and an upper layer of inorganic-organic perovskite ($CH_3NH_3PbI_3$). Similarly, the model (B) had the same structure and materials, but the upper layer was made of GaN, as shown in figure 2. Likewise, model (C) had the same structure and materials, but the upper layer was made of GaAs, as shown in figure 3. In addition, the silicon layer dimensions 50x50x10 μm, the indium sphere has a radius of 12 μm, and the upper layer ($CH_3NH_3PbI_3$, GaAs, GaN) dimensions $50x50x5\ \mu m$. These dimensions are chosen to represent the RVE of the entire structure, as shown in figures 1-3. Furthermore, the indium sphere was located at a

depth of 5 μm within the silicon layer, while the $CH_3NH_3PbI_3$, GaAs and GaN layers had a depth of 2.5 μm.

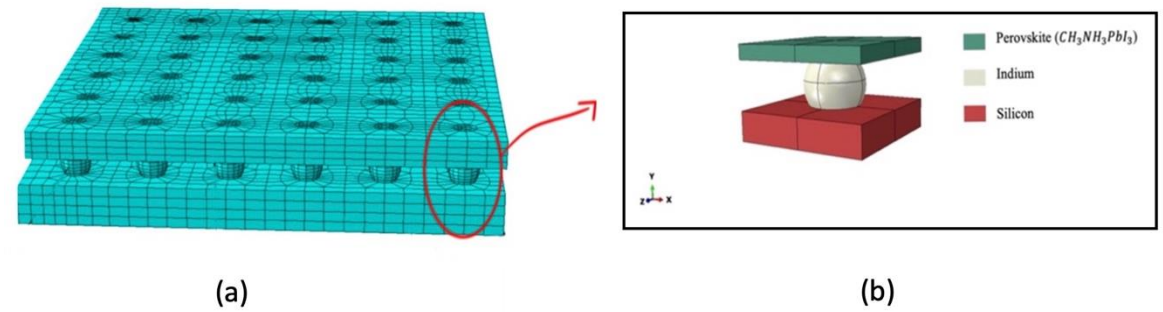

Figure 1. Geometry and the MJPV cell; (a) represents MJPV cell for model (A); (b) represents the RVE for model (A).

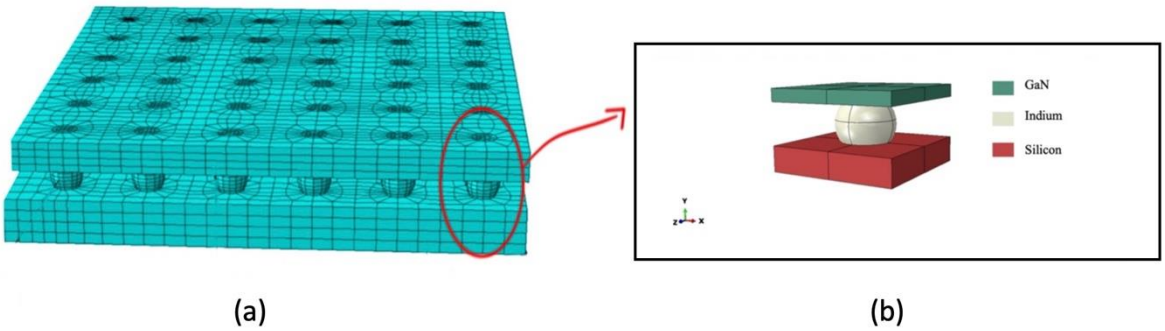

Figure 2. Geometry and the MJPV cell; (a) represents MJPV cell for model (B); (b) represents the RVE for model (B).

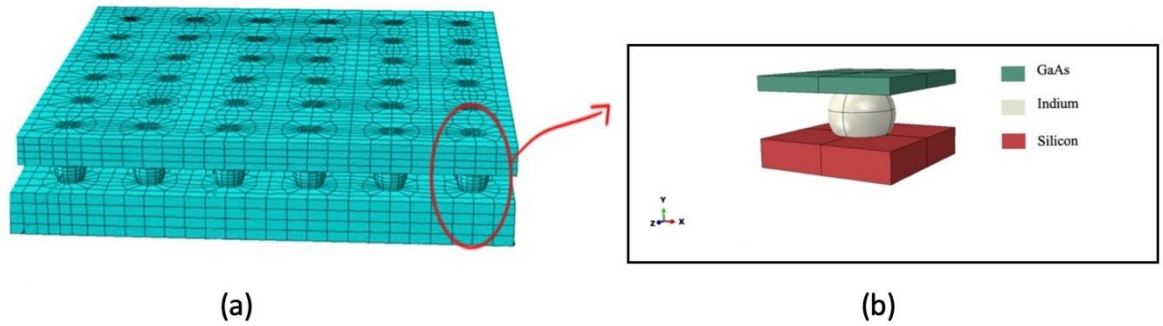

Figure 3. Geometry and the MJPV cell; (a) represents MJPV cell for model (C); (b) represents the RVE for model (C).

The following figure 4 shows the boundary conditions applied at the nodes located at the outer edge of the 3D structure. Moreover, symmetric planes in X and Z axis are used to apply symmetric boundary conditions to the models and the Hexahedral meshing type used for the 3D structure for more accuracy with meshing size 2.5.

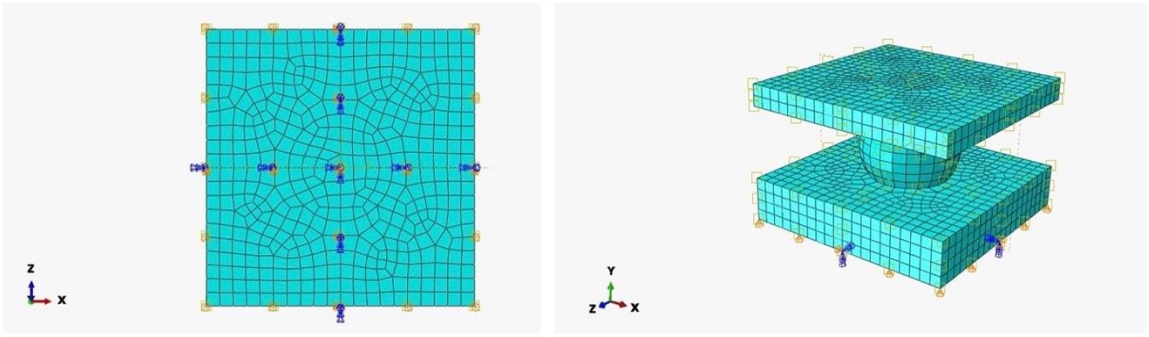

Figure 4. Boundary conditions for the three models:(a) bottom view for the RVE; (b) isometric view for the RVE.

The material deformation can be known from the stress σ, strain $\dot{\varepsilon}$, homologous temperature T_h (T_h=T/T_m) in kelvin unit, and the microstructure (such as the grain size, impurities) of the material. Usually, the material react under specific conditions could be detect via the flow law associated with more than one mechanism. The Duhamel-Neumann thermoelastic constitutive law applied to the 3D structure that account the thermal stresses, to check the model behaviour under different temperatures [28].

$$\sigma_{ij} = C_{ijkl}\varepsilon_{kl} - \beta_{ij}(T - T_0) \quad (1)$$

Where:

- σ: the second order Cauchy stress tensor.
- ε: the second order linearized strain tensor.
- β: the second order thermoelastic moduli tensor.
- C: the fourth order elasticity tensor.
- T: the current temperature.
- T_0: the reference temperature.

The second step after running the thermoelastic model is to apply uniform temperature to 3D structure in order to simulate the thermal stresses happened during the fabrication and operation process of the perovskite or GaAs or GaN/Silicon. The model's initial temperature is set at 423 K, subsequently cooled to room temperature at 300 K, with mid-heating and final heating temperatures of 330 K and 358 K, respectively, applied in the simulation[29,30].

As aforementioned that the substrate layer in model A, B, C was made from silicon which is an isotropic material and the same behaviour for the GaAs, GaN, and indium. Given that the indium junction or sphere exhibits greater ductility than the silicon layer, it is predicted that the materials employed in multijunction photovoltaic cells (MJPVs) maintain elasticity during the entire process. Additionally, for each of the aforementioned materials, Poisson's ratio, Young's modulus, and the thermal expansion coefficient are considered, as the material behaviour is isentropic. Moreover, when crystalline silicon exhibiting isotropic behaviour is applied to the generic thermoelastic model, it simplifies to the following equation:

$$\sigma_{ij} = \lambda\varepsilon_{kk}\delta_{ij} + 2\mu\varepsilon_{ij} - (3\lambda + 2\mu)\alpha(T - T_0)\delta_{ij} \quad (2)$$

Where:

- λ: Lame's constant.
- μ: the shear modulus.
- δ_{ij}: the Kronecker delta (replacement operator).
- α: the coefficient of linear thermal expansion.

The fourth order elastic tensor of $CH_3NH_3PbI_3$ crystals with independent elastic coefficients and tetragonal symmetry below 330 K is [31]:

$$[C] = \begin{pmatrix} 20.1 & 14.6 & 6.8 & 0 & 0 & 0 \\ & 20.1 & 6.8 & 0 & 0 & 0 \\ & & 17.9 & 0 & 0 & 0 \\ & & & 1.6 & 0 & 0 \\ & & \text{Sym} & & 1.6 & 0 \\ & & & & & 9.2 \end{pmatrix} (\text{GPa}) \quad (3)$$

Both the Silicon and perovskite GaAs, GaN layers are assumed to have isotropic thermal effects. As a result, β_{ij} is reduced to the isotropic tensor of second order (α_{ij}) and becomes [29]:

$$\alpha_{ij} = \alpha(T - T_0)\delta_{ij} \quad (4)$$

As a result, the second order thermal strain tensor (ε_{ij}^T) is:

$$\varepsilon_{ij}^T = \alpha_{ij}(T - T_0) \quad (5)$$

Meanwhile, the following equations are used to calculate the Von Mises stress (σ^e) generated on the structure:

$$\sigma^e = \frac{3}{\sqrt{2}}\tau^{Oct} \quad (6)$$

$$\tau^{Oct} = \frac{1}{3}\sqrt{(2\,I_1^2 - 6\,I_2)} \quad (7)$$

$$I_1 = tr(\sigma) \quad (8)$$

$$I_2 = \frac{1}{2}\left(I_1^2 - tr(\sigma^2)\right) \quad (9)$$

Where:

- τ^{Oct}: the shear stress on the octahedral plane.
- I_1, I_2: the Cauchy stress tensor invariants.

Furthermore, the following table 1 illustrate the parameter used in the software for each material.

Table 1. Constants Parameter for Each Material [18,29–31][18,32–35].

Parameters	Unit	CH_3 NH_3 PbI_3	Silicon	Indium	GaAs	GaN
Young's modulus (E)	GPa	-	168.9	14	144	330
Poisson's ratio (v)	-	-	0.262	0.46	0.31	0.23
α (k-1) x10-6	k-1	43	2.6	33	5.8	3.17

Usually the Periodic Boundary Conditions (PBCs) are a group of boundary condition that apply to Representative Volume Element (RVE) or a Statistical Volume Element (SVE), in order to simulate a large (infinite) system. However, the PBCs are not applied to the models that has a torsion and bending loads. Therefore, in this present work Extended Periodic Boundary Conditions (xPBCs) are applied to the models in order to overcome the limitation existing in the Periodic boundary conditions such as the bending and torsion load that already exist in the present 3D structure. The effect of curvature, such as in bending, cannot be accurately represented by employing a constant average strain. The strain along the axis connecting the master and slave surfaces is graphed versus the other two axes, and this constraint is alleviated to render the plot planar. This ensures periodicity while being more comprehensive, as the xPBCs equations are fulfilled by the solution to the traditional PBCs equations. The illustration of node pairing in the xPBCs is presented in figure 5. The PBCs

equations are utilised between any two pairings in conventional PBCs, associating each node on the master surface (ABCD) with its equivalent node on the slave surface (A'B'C'D'). To avert the occurrence of four initially collinear nodes and to generate a straightforward set of equations, xPBCs confines the first three node pairs to possess star-shaped configurations [36].

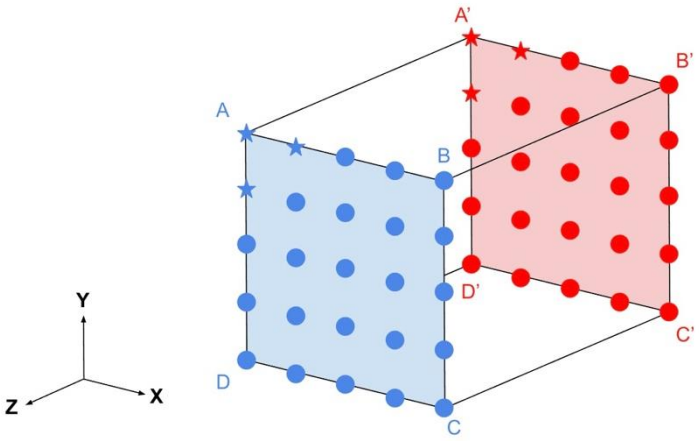

Figure 5. Example of node pairing for xPBCs, with blue designating the master surface and red the slave surface [36]

3. Results

A cross-section of three different models demonstrating the internal and external stress distribution. The indium segment exhibits the maximum stress concentration (average stress of 41 MPa), followed by silicon with lower stress levels (average stress of 27.4 MPa), while the perovskite section demonstrates the least stress accumulation (average stress of 3.4 MPa), as illustrated in figure 6. The indium junction/sphere undergoes slight distortion from the sides due to the considerable temperature disparity between the indium and silicon.

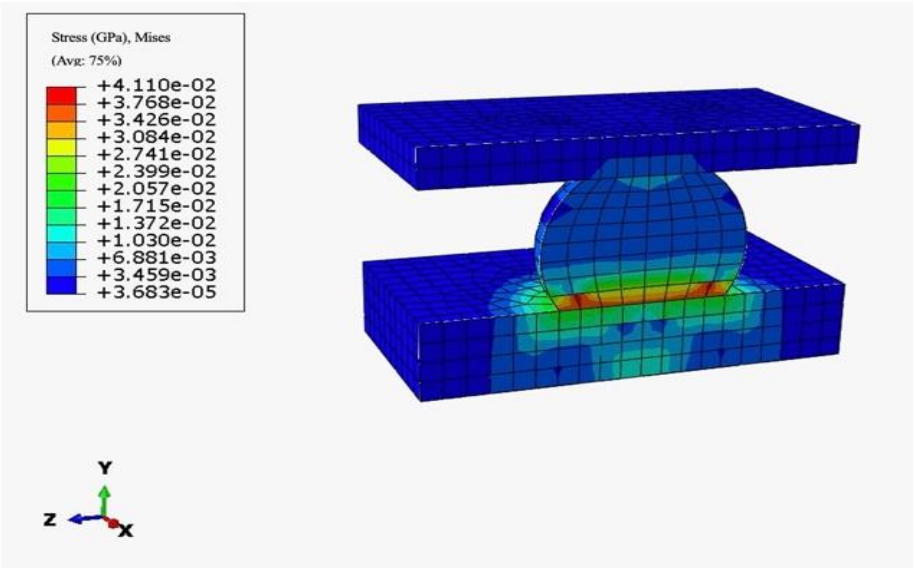

Figure 6. The thermal stress distribution on model (A).

Figure 7 illustrates the average stress for model B, revealing that the GaN region exhibits the largest stress concentration (average stress of 45.5 MPa), but the thermal stresses in the indium and silicon portions are equivalent to those in model A.

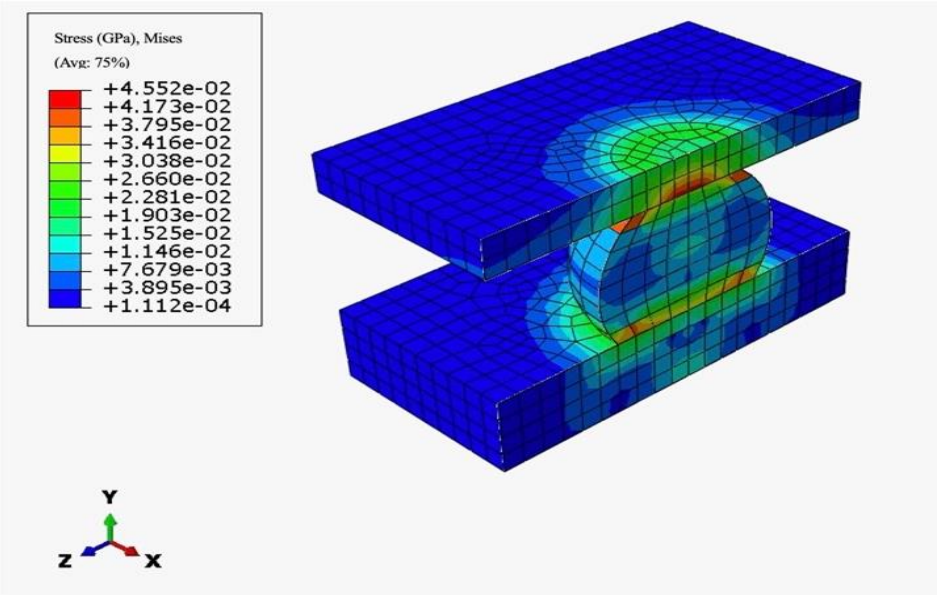

Figure 7. The thermal stress distribution on model (B).

Figure 8 illustrates that the average stress for model C indicating that the GaAs section exhibits the highest stress concentration (average stress of 48 MPa), while the thermal stress in the indium section rises to 44.5 MPa, and the average stress for silicon experiences a slight increase to 28 MPa. The cause of the increased stress is the significant temperature mismatch between GaAs and silicon.

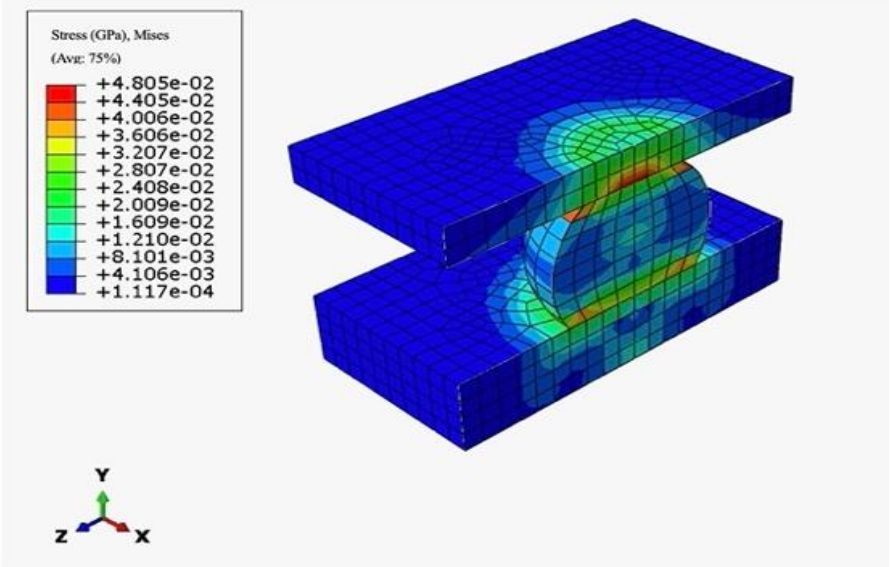

Figure 8. The thermal stress distribution on model (C).

Table 2 illustrates a quantitative comparison of thermal stress between the proposed Multijunction Photovoltaic Cells (MJPVs) models and previous studies, but across different MJPV configurations. It is noteworthy that the use of an embedded void approach (EVA) in MJPVs might yield dual effects either increasing or decreasing thermal stresses, dependent upon the density and positioning of the voids. Furthermore, the thermal stress values for the proposed model differ from those in prior studies, as the proposed model incorporates three junctions and includes distinct interface zones. For instance, the current study examines the interfaces between indium/Si, indium/GaAs, indium/GaN, and indium/perovskite, whereas previous studies focused on the interfaces of GaN/Si or GaAs/Si.

Table 2-comparison analysis of thermal stress in Multijunction Photovoltaic Cells (MJPVs) with and without Embedded Void Approach (EVA).

System	Tool	Result	Exp./Num.	Ref.
GaN/Si-MJPVs with EVA	ABAQUS	Stress: 653 MPa	Numerical	[37]
GaN/Si-MJPVs without EVA	ABAQUS	Stress: 1.4 GPa	Numerical	[37]
GaN/Si-MJPVs without EVA	ABAQUS	Stress: 1.4 GPa	Experimental	[38]
GaAs/Si-MJPVs with EVA	ABAQUS	Si layer: 79.5 MPa, GaAs layer: 186 MPa	Numerical	[18]
GaAs/Si-MJPVs without EVA	ABAQUS	Si layer: 108 MPa, GaAs layer: 173 MPa	Numerical	[18]
Model A (Current Study)	ABAQUS	Indium: 41 MPa, Si: 27.4 MPa, Perovskite: 3.4 MPa	Numerical	Current study
Model B (Current Study)	ABAQUS	Indium: 41 MPa, Si: 27.4 MPa, GaN: 45.5 MPa	Numerical	Current study
Model C (Current Study)	ABAQUS	Indium: 44.5 MPa, Si: 28 MPa, GaAs: 48 MPa	Numerical	Current study

As aforementioned, all the models are exposed to the same temperature range, but the thermal stresses that occurred in each model are different, and the reason beyond that is the difference between the thermal expansion coefficient for each material, especially at the intersection zone. For instance, in model A, there is no high thermal stress or red zone in the intersection between the indium and perovskite, as the thermal expansion coefficient for the two materials is close. In contrast, high thermal stresses happened in the intersection zone between the indium and GaAs as a result of the large difference in the thermal expansion coefficients.

4. Conclusion

The growth of renewable energy sources has become an essential focus recently, with solar energy presenting a viable alternative to conventional fossil fuels. Photovoltaic (PV) cells are essential for capturing solar energy and turning it into usable power, with the primary aim of solar cell research being the enhancement of the long-term energy production of PV systems. This study proposed three different models for MJPV cells in order to discover the thermal stress for perovskite, GaAs, and GaN upper layers with silicon as a substrate and indium spheres as middle junctions. The comparison of findings from the three models clearly indicates that models (A) and (B) exhibited much lower thermal stresses at all junctions compared to model (C), along with reduced deformation at the upper junction. This is likely due to the three models being constructed from distinct materials. The peak stress is observed in model (B), particularly within the GaAs upper layer. Overall, the three models have the potential to achieve higher efficiency than the other single-junction solar cells. Future research will investigate the impact of various thermal configurations in the context of solar panel operating conditions, aiming to mitigate dislocation propagation resulting from elevated thermal stresses via the Embedded Void Approach (EVA).

Acknowledgments

I would like to express my deepest gratitude to Prof. Iman El-Mahallawi for her invaluable support, guidance, and supervision throughout this study. Her insightful feedback and expertise in the field were instrumental in shaping and structuring this research.

References

[1] Masuko K, Shigematsu M, Hashiguchi T, Fujishima D, Kai M, Yoshimura N, Yamaguchi T, Ichihashi Y, Mishima T, Matsubara N, Yamanishi T, Takahama T, Taguchi M, Maruyama E and Okamoto S 2014 Achievement of more than 25% conversion efficiency with crystalline silicon heterojunction solar cell *IEEE J Photovolt* **4**

[2] Kayes B M, Nie H, Twist R, Spruytte S G, Reinhardt F, Kizilyalli I C and Higashi G S 2011 27.6% Conversion efficiency, a new record for single-junction solar cells under 1 sun illumination *Conference Record of the IEEE Photovoltaic Specialists Conference*

[3] Würfel P 2007 *Physics of Solar Cells: From Principles to New Concepts*

[4] King R R, Law D C, Fetzer C M, Sherif R A, Edmondson K M, Kurtz S, Kinsey G S, Cotal H L, Krut D D, Ermer J H and Karam N H 2005 Pathways To 40 % -Efficient Concentrator Photovoltaics *20th European Photovoltaic Solar Energy Conference*

[5] Meier J, Dubail S, Golay S, Kroll U, Fay S, Vallat-Sauvain E, Feitknecht L, Dubail J and Shah A 2002 Microcrystalline silicon and the impact on micromorph tandem solar cells *Solar Energy Materials and Solar Cells* **74**

[6] Jeong W S, Lee J W, Jung S, Yun J H and Park N G 2011 Evaluation of external quantum efficiency of a 12.35% tandem solar cell comprising dye-sensitized and CIGS solar cells *Solar Energy Materials and Solar Cells* **95**

[7] Barber G D, Hoertz P G, Lee S H A, Abrams N M, Mikulca J, Mallouk T E, Liska P, Zakeeruddin S M, Grätzel M, Ho-Baillie A and Green M A 2011 Utilization of direct and diffuse sunlight in a dye-sensitized solar cell - Silicon photovoltaic hybrid concentrator system *Journal of Physical Chemistry Letters* **2**

[8] Qin W, Yu W, Zi W, Liu X, Yuan T, Yang D, Wang S, Tu G, Zhang J, Liu F S and Li C 2014 High efficiency organic/a-Si hybrid tandem solar cells with complementary light absorption *J Mater Chem A Mater* **2**

[9] Yankson E 2021 The ILA study group on the Role of Cities in International Law City Report: Arusha *International Law Associatiion*

[10] Zhao Y, Datta K, Phung N, Bracesco A E A, Zardetto V, Paggiaro G, Liu H, Fardousi M, Santbergen R, Moya P P, Han C, Yang G, Wang J, Zhang D, Van Gorkom B T, Van Der Pol T P

A, Verhage M, Wienk M M, Kessels W M M, Weeber A, Zeman M, Mazzarella L, Creatore M, Janssen R A J and Isabella O 2023 Optical Simulation-Aided Design and Engineering of Monolithic Perovskite/Silicon Tandem Solar Cells *ACS Appl Energy Mater* **6**

[11] Cotal H, Fetzer C, Boisvert J, Kinsey G, King R, Hebert P, Yoon H and Karam N 2009 III-V multijunction solar cells for concentrating photovoltaics *Energy Environ Sci* **2**

[12] Yamaguchi M, Takamoto T, Araki K and Ekins-Daukes N 2005 Multi-junction III-V solar cells: Current status and future potential *Solar Energy* **79**

[13] Yang W S, Noh J H, Jeon N J, Kim Y C, Ryu S, Seo J and Seok S Il 2015 High-performance photovoltaic perovskite layers fabricated through intramolecular exchange *Science (1979)* **348**

[14] Zhang X, Ren X, Liu B, Munir R, Zhu X, Yang D, Li J, Liu Y, Smilgies D M, Li R, Yang Z, Niu T, Wang X, Amassian A, Zhao K and Liu S 2017 Stable high efficiency two-dimensional perovskite solar cells via cesium doping *Energy Environ Sci* **10**

[15] Camarchia V, Quaglia R, Ramella C and Pirola M 2017 Power amplifier MMICs for 15 GHz microwave links in 0.25 üm GaN technology *Proceedings of the 2017 International Workshop on Integrated Nonlinear Microwave and Millimetre-Wave Circuits, INMMiC 2017*

[16] Salah S I, Hatem T M, Khalil E E and Bedair S M 2019 Embedded void approach effects on intrinsic stresses in laterally grown GaN-on-Si substrate *Materials Science and Engineering: B* **242**

[17] Salah S I, Hatem T M, Khalil E E, Abdelmaksoud W A and Bedair S M 2017 Embedded void approach for nitride based multi-junction photovoltaic cells *AIAA SciTech Forum - 55th AIAA Aerospace Sciences Meeting*

[18] Hatem T, Elewa M and Salah A 2014 MICROSTRUCTURAL MODELING OF INTRINSIC STRESSES IN MULTI-JUNCTION BASED PHOTOVOLTAIC *The International Conference on Applied Mechanics and Mechanical Engineering* **16**

[19] Bagheri S, Talebzadeh R, Sardari B and Mehdizadeh F 2019 Design and simulation of a high efficiency InGaP/GaAs multi junction solar cell with AlGaAs tunnel junction *Optik (Stuttg)* **199**

[20] Tucher N, Höhn O, Goldschmidt J C and Bläsi B 2018 Optical modeling of structured silicon-based tandem solar cells and module stacks *Opt Express* **26**

[21] Eisenlohr J, Lee B G, Benick J, Feldmann F, Drießen M, Milenkovic N, Bläsi B, Goldschmidt J C and Hermle M 2015 Rear side sphere gratings for improved light trapping in crystalline silicon single junction and silicon-based tandem solar cells *Solar Energy Materials and Solar Cells* **142**

[22] Liu Z, Ren Z, Liu H, Mailoa J P, Sahraei N, Siah S C, Sofia S E, Lin F, Buonassisi T and Peters I M 2015 Light management in mechanically-stacked GaAs/Si tandem solar cells: Optical design of the Si bottom cell *2015 IEEE 42nd Photovoltaic Specialist Conference, PVSC 2015*

[23] Sai H, Kanamori Y, Arafune K, Ohshita Y and Yamaguchi M 2007 Light trapping effect of submicron surface textures in crystalline Si solar cells *Progress in Photovoltaics: Research and Applications* **15**

[24] Gee J M 2002 Optically enhanced absorption in thin silicon layers using photonic crystals *Conference Record of the IEEE Photovoltaic Specialists Conference*

[25] Dewan R and Knipp D 2009 Light trapping in thin-film silicon solar cells with integrated diffraction grating *J Appl Phys* **106**

[26] Zandi S and Razaghi M 2019 Finite element simulation of perovskite solar cell: A study on efficiency improvement based on structural and material modification *Solar Energy* **179** 298–306

[27] Vaillon R, Parola S, Lamnatou C and Chemisana D 2020 Solar Cells Operating under Thermal Stress *Cell Rep Phys Sci* **1**

[28] Simo J C and Marsden J E 1984 On the rotated stress tensor and the material version of the Doyle-Ericksen formula *Arch Ration Mech Anal* **86**

[29] Bett A J, Schulze P S C, Winkler K, Gasparetto J, Ndione P F, Bivour M, Hinsch A, Kohlstädt M, Lee S, Mastroianni S, Mundt L E, Mundus M, Reichel C, Richter A, Veit C, Wienands K, Würfel U, Veurman W, Glunz S W, Hermle M and Goldschmidt J C 2017 Low temperature perovskite solar cells with an evaporated TiO2 compact layer for perovskite silicon tandem solar cells *Energy Procedia* vol 124

[30] Rakita Y, Cohen S R, Kedem N K, Hodes G and Cahen D 2015 Mechanical properties of APbX3 (A = Cs or CH3NH3; X = i or Br) perovskite single crystals *MRS Commun* **5**

[31] Sadd M H 2004 *ELASTICITY: Theory, Applications, and Numerics*

[32] Luque A and Hegedus S 2011 *Handbook of Photovoltaic Science and Engineering*

[33] Jacobsson T J, Schwan L J, Ottosson M, Hagfeldt A and Edvinsson T 2015 Determination of Thermal Expansion Coefficients and Locating the Temperature-Induced Phase Transition in Methylammonium Lead Perovskites Using X-ray Diffraction *Inorg Chem* **54**

[34] Morkoç H 2008 *Handbook of Nitride Semiconductors and Devices Vol. 1: Materials Properties, Physics and Growth* vol 1

[35] Maniatty A and Karvani P 2015 Constitutive relations for modeling single crystal GaN at elevated temperatures *Journal of Engineering Materials and Technology, Transactions of the ASME* **137**

[36] Ibrahima M and Hatema T Extended Periodic Boundary Condition (xPBC) *submitted to Applied Physics Letters*

[37] Salah S I, Hatem T M, Khalil E E and Bedair S M 2019 Embedded void approach effects on intrinsic stresses in laterally grown GaN-on-Si substrate *Materials Science and Engineering: B* **242**

[38] Cheng J, Yang X, Sang L, Guo L, Zhang J, Wang J, He C, Zhang L, Wang M, Xu F, Tang N, Qin Z, Wang X and Shen B 2016 Growth of high quality and uniformity AlGaN/GaN heterostructures on Si substrates using a single AlGaN layer with low Al composition *Sci Rep* **6**